Measurement of the Appearance and Growth of Tow Buckling Defect in the Frame of Complex Shape Manufacturing Process by Using Fringe Projection Technique

— Source link ↗

Pierre Ouagne, Damien Soulat, Christophe Tephany, Jean Gillibert

Institutions: University of Orléans, ENSAIT

Related papers:

- Experimental preforming of highly double curved shapes with a case corner using an interlock reinforcement

- Complex shape forming of flax woven fabrics: Design of specific blank-holder shapes to prevent defects

- Variability, fibre waviness and misalignment in the determination of the properties of composite materials and structures

- Meso modelling for composite preform shaping – Simulation of the loss of cohesion of the woven fibre network

- Effect of inter-ply sliding on the quality of multilayer interlock dry fabric preforms

Any correspondence concerning this service should be sent
to the repository administrator: tech-oatao@listes-diff.inp-toulouse.fr

Measurement of the Appearance and Growth of Tow Buckling Defect in the Frame of Complex Shape Manufacturing Process by Using Fringe Projection Technique

P. Ouagne*, D. Soulat†, C. Tephany* and J. Gillibert*

*University of Orléans, PRISME EA4229, F-45072, Orléans, France
†GEMTEX, ENSAIT, Roubaix 2 allée Louise et Victor Champier, 59056, Roubaix, France

ABSTRACT: During the manufacturing of composite complex shape parts, defects such as tow buckles characterised by out of plane elevation may appear. The parameters controlling the appearance and growth of the defect are not completely understood and need to be investigated. A device capable of reproducing tow buckles has been used to study the tow buckling phenomenon. Several techniques able to measure out of plane elevations are discussed to detect the appearance and evaluate continuously the growth of the tow buckle in relation to its size and shape. The fringe projection technique was chosen as it gives the best compromise between the size of the defect to measure and its resolution.

If the in-plane bending angle is the main criterion at the origin of the tow buckle appearance and growth, it is not the only one. This work shows that the fabric architecture such as the space between the tows perpendicular to the one showing the buckle is also crucial to control the buckle's appearance and growth. It also shows that the differential bi-axial loading of the fabric as well as the stiffness of the tows in the three main directions greatly influences the appearance of the defect.

KEY WORDS: *complex shape, composite manufacturing processes, fringe projection, textile forming, tow buckling, woven fabric*

Introduction

During the manufacturing process, defects may occur in composite parts. Potter *et al.* [1] have presented a list of defect states that may occur during the composite manufacturing processes. Some of the defects appearing during the first step of the RTM process (preforming stage) may have adverse impacts on the performance of composite parts and should be prevented [2, 3]. At the scale of the preform, denoted macroscale, it is possible to investigate if the preform shape is well obtained, if wrinkles appear, if there is non-homogeneity of the fibre density in tows, or if a discontinuity of the preform due to sliding of tows takes place [4–8]. At this scale, a lot of studies [9–15] have been published on the use of full field optical measurements of strains. They provide an ideal instrument to quantify the strain levels in different deformation modes (tension, in-plane shear). At the scale of the tows, mesoscale, other defects may appear. Tow misalignment in the plane of the fabric, [1] or out-of-plane misalignment also called tow buckles [4, 16, 17], can be investigated. All these defects have a strong influence on the resin flow impregnation because they modify the in-plane and through-the thickness permeability components [18–22], and they probably impact the performance of the composite part because the fibres are not aligned anymore. In the case of the fibre waviness defect that may also lead to out of plane bending of tows, Bloom *et al.* and Davidson *et al.* showed

that a 40% knock-down in strength was observed in the case of severe waviness [4, 23, 24]. Hayman *et al.* also reported that fibre waviness has for effect to reduce the compression properties of a sandwich material by 55%. The misalignment defect such as fibre waviness has therefore serious consequences on the mechanical properties of the final composite material. In the case of the tow buckle defect, no study reported specifically their effect on the composite mechanical properties. However, one can observe that the tow buckles has for consequence to impose fibre misalignment that has serious consequences on the composite strength as mentioned right above in this paragraph.

By working on the forming process, Ouagne *et al.* and Capelle *et al.* [16, 17] showed that the appearance of this defect depends on multiple criteria. They manage during their studies to prevent or limit the buckles appearance by working on the reinforcement architecture and on the forming process parameters.

If some experimental work has already been carried out on the reduction or on the prevention of the buckles occurrence, all the parameters controlling the buckles appearance have not been yet identified with accuracy. By analogy with the wrinkling defect or pull-out defects, which have been widely studied, this work proposes to study independently of the preforming process the tow or yarn buckling defect. Indeed, a lot of work has been devoted to study the relationship between the in-plane shear

phenomenon and the appearance of the wrinkling defect mainly caused by the locking of warp and weft yarns [23, 24]. During the forming process, the appearance of wrinkling is not only due to in-plane shear but also to the tension of the membrane and the bending stiffness. Several authors therefore decided to study independently of the process this defect by designing specific in-plane shear characterisation protocols using either the bias extension test or the picture frame test [1, 14, 25–29]. Some other authors proposed different approach to model the appearance of defects such as the wrinkling defect [30–33]. Kirkwood *et al.* [34] also used the same approach to study independently of the process the yarn pull-out phenomenon by designing an especially dedicated set-up.

Non-destructive evaluation (NDE) techniques have been employed to inspect and characterise composite structures [28]. Various NDE methods, such as the optical techniques of holography, electronic speckle-pattern interferometry, shearography and time-domain moiré interferometry, are used for thermoplastic or thermoset composites and are described by a number of authors [35–41]. These techniques provide wide-area qualitative imagery in the in- and out-of-plane displacement at the surface of a structure. However, their effectiveness at inspecting structures of any significant thickness for buried defects is normally vastly reduced [42]. If the use of all these methods is well described for composite parts, the detection of defects at the scale of fabrics, before injection of resin, and associated to this preforming stage, has not really been studied.

In this paper, an experimental device to reproduce the tow buckling phenomenon is used and is associated to the fringe projection technique to quantify the out-of-plane defect.

Design of the Instrumented Tow Buckling Device

Up to date knowledge on the tow buckle generation

The bending of tow in its plane has already been studied in the frame of the robot lay-up of pre-impregnated ribbons. Beakou *et al.* [43] modelled the appearance of such defects. However, the appearance of tow buckles in woven fabrics is more complex. In the first studies reporting the appearance of the tow buckling defect during the forming process, the main mechanism without which the tow buckling defect cannot appear has been identified for different carbon, glass and flax-based flat tow woven fabrics by several authors. One of the first descriptions was given by Harrison *et al.* in 2002 [29]. This work was more recently completed by some pieces of work performed at Orléans [8, 16, 17]. This mechanism is the bending in their plane of flat tows imposed by the geometry of the shape (Figure 1).
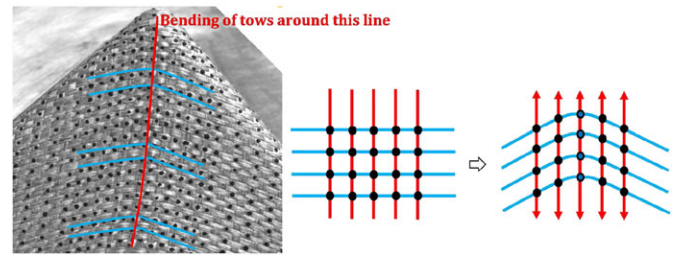

Figure 1: Bending in their plane of tows

As this mechanism cannot be or can only be partially accommodated, another mechanism consisting in deforming the tow out of its plane takes place and a tow buckle appears as shown in Figure 2.

The measurements performed on a face of a tetrahedron where tow buckling appears show that globally, the bending angles remain similar all along the buckling zone with lower values (more severe bending) towards the top of the shape [16]. This bending angle quasi-continuity means that the displacements of the tows exhibiting the buckles are almost similar and symmetrical against the curvature point line. This mechanism is the same as the one observed for ribbon lay-up.

However, the in-plane bending of the tow is not the only parameter influencing the appearance of the tow buckles. Reducing the tension of the tows perpendicular to the ones exhibiting the buckles delays and reduces the size of the buckles to a very low extent [17]. This is particularly true for the tetrahedron shape where the tension is maximum in the zone exhibiting buckles. As a consequence, the device should be able to impose different in-plane bending angles to the tow showing the buckles and to apply different magnitudes of tension to the perpendicular tows. Other parameters related to the meso and macro architecture of the fabric are also very important and should be studied with the device. The device should therefore permit the study of different types of reinforcement with different yarn or tow architectures and geometries.
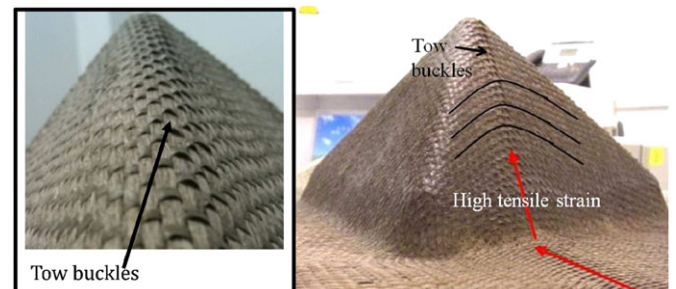

Figure 2: Tow buckles on an edge and on a face of a tetrahedron shape

The tow buckling device

According to the previous section, the buckling defect is mainly the result of a combination between the bending of tows in their plane and level of tension applied to the tows perpendicular to the ones showing the buckles. The tension imposed to the tows showing the buckles is also probably very important and should also be studied. A device has therefore been designed to impose separately in-plane bending angles to the tows showing the buckles and variable tensions in the perpendicular tows. The design of the mechanical part of the device was described into details in [44] and is summarised in Figure 3. The fabric samples are maintained by jaws in the horizontal and vertical directions. Adjustable tensions can be applied in both directions. In Figure 3a, the horizontal jaws can bend in their plane following a circular translation so that the tows bend on a given point and stay straight as shown in Figure 1. To perform the circular translation, the deformable parallelogram technique has been used (Figure 3b).

Semi-cross geometry samples have been chosen as these ones prevent the appearance of wrinkles or tow sliding on the contrary of square samples or cross shape samples, respectively. The device is instrumented. Load sensors, Linear Variable Differential Transformer, optical measurements using mark tracking technique and fringe projection measurement techniques are used during the test to provide all the necessary information required to study the tow buckling phenomenon. The device instrumentation is summarised in Figure 4.

Measurement of the buckle's height

The detection of the buckles appearance and the measurement of its amplitude variation during its growth are critical parameters that need to be carefully and accurately measured. Particularly, the buckle's size, or buckle's height (Figure 5) should be evaluated by a non-contact technique to avoid any interaction between the measurement and the buckle's appearance and growth.

The determination of the buckle's height consists in evaluating the topography of the reinforcement at given times during a test. As an example, the size of the buckle should be measured during the test for any modification of a device parameter such as the bending angle, or the tension applied on the tows in each direction. As a consequence, the measurement tool should be able to scan a relatively large zone on the surface of the sample test, and the acquisition and treatment times should be reasonable.

Several methods were investigated to measure this parameter. The first one is the stereo-image correlation with 3D mark tracking, which permits to evaluate the displacement field of the reinforcement [10, 44]. However, this method was rejected as it is not possible to follow the marks through the totality of the test because of the incidence angle of the cameras. This is due to the fact that during the appearance of the buckles, some zones of the fabric, visible at the beginning of the test cannot be observed at the end of the test, and the profile of the buckles cannot be entirely recorded. The second tested method is the shadow detection method. It consists in observing the
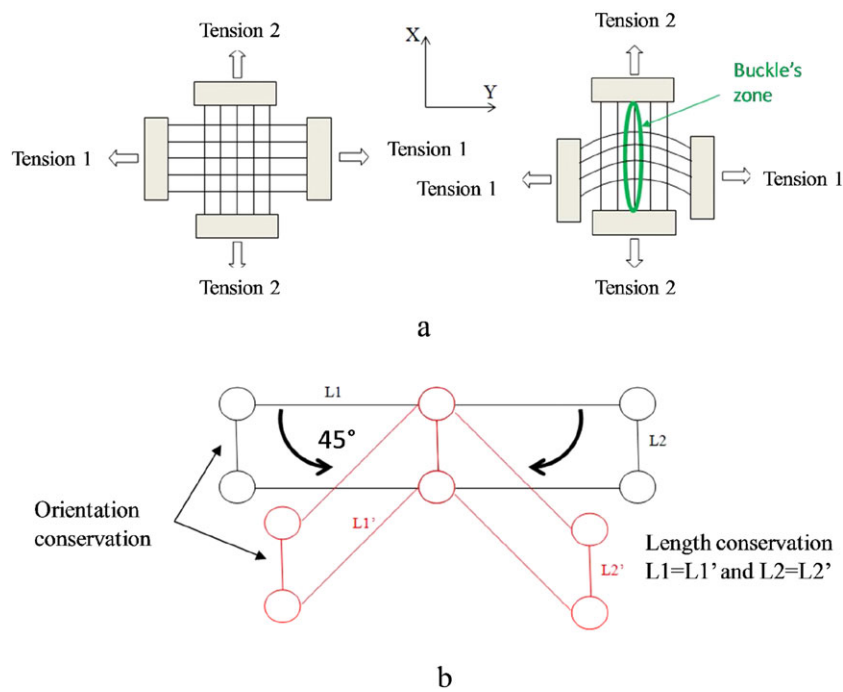

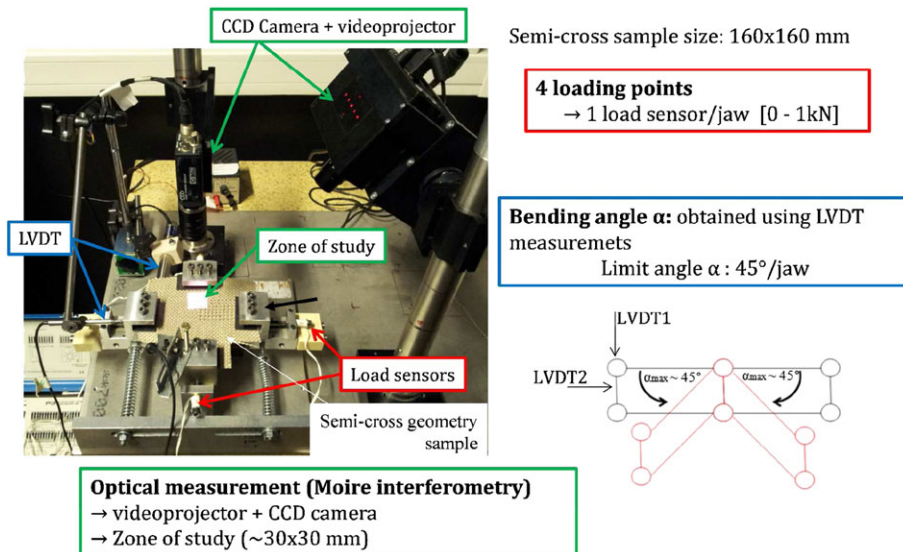**Figure 3:** Principle of the tow buckling device

Figure 4: Instrumentation of the tow buckling device

evolution of the size of the shadows caused by the buckle's appearance under glancing light conditions. If this method could be easily used for the determination of the profile of a unique buckle, the profile of the shadow during the test is disturbed by the elevation of adjacent buckles. The evaluated buckle's size is therefore not representative of the true height of the defect. This method was also rejected.

The third tested method is fringe projection. This method is particularly interesting for our case of study because it permits to measure the topography of the surface of an object without any contact, which could modify the state of the surface [45–48]. Moreover, its resolution and zone of study correspond to the requirements of this work. Table 1 compares the resolution and extent of the zone of study of different interferometry methods and the Fringe projection techniques. The fringe projection technique is also particularly interesting as it does not necessitate that the material is conductor (scanning tunnel microscopy or scanning electron microscopy), and the size of the observation zone is much larger than the one of atomic force microscopy, which requires long acquisition times.

In our case of study, the size of the buckles is situated in a range between 0 and 1.5 mm. The use of fringe projection is therefore the most appropriated technique. The global

principle and the performance of this measurement technique were reviewed by Gorthi *et al.* [49], and no further description will be given in this paper.

Experimental Procedure

Description of the used fringe projection apparatus

The measurements performed by using the fringe projection technique have been completed at the Science et Ingéniérie des Matériaux et Procédés of Grenoble (http://simap. grenoble-inp.fr/accueil/). The used experimental device is composed of three main elements: a CCD camera, a video projector and software elements H3SensorDigit3D coupled to the FringeAnalysis4®. The H3SensorDigit3D is a piece of software developed by the HOLO3 Company (Saint Louis, France) dedicated to the 3D digitalisation using optical ways. The FringeAnalysis4® is a software dedicated to the analysis of fringes images used in the holography, speckle or structured light interferometry. A video projector is used to project calibrated computer elaborated fringes.

Materials

The flax fabric used in this study is a plain-weave fabric with an areal weight of $280 \pm 19\,g/m^2$, manufactured by Groupe Depestele (France) from untwisted tows. The fabric is not balanced, as the space between the weft tows $(1.59 \pm 0.09\,mm)$ is different from the one between the warp tows $(0.26 \pm 0.03\,mm)$. The width of the warp and the weft tows are respectively $2.53 \pm 0.12\,mm$ and $3.25 \pm 0.04\,mm$. As a consequence, there are 360 warp tows and 206 weft tows per metre of fabric.
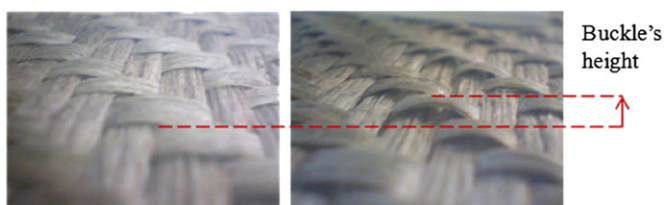

Figure 5: Definition of the buckle height

Table 1: Dimensional characteristics of different topography measurement techniques [48]

	Real time holography	Dynamic holography	TV-holography	Speckles	Fringe projection
Surface of analysis	$16\,cm^2–1\,m^2$	$16\,cm^2–10\,m^2$	$10\,mm^2–1\,m^2$	$25\,mm^2–1\,m^2$	$100\,mm^2–1\,m^2$
Measurement range extent	$0.1–20\,\mu m$	$0.1–20\,\mu m$	$0.1–10\,\mu m$	$0.1–10\,\mu m$	several centimetres
Resolution for displacement measurements	$0.01\,\mu m$	$0.01\,\mu m$	$0.1\,\mu m$	$0.1\,\mu m$	$0.1–0.4\,mm$

Test conditions

In this work, the initial tensions in the X and Y directions are imposed by the device. They are fixed to low values, (8 and 15.3 N, respectively).

Results

Initial test: profile and size of the buckles at the initial and final states

The profile of altitude studied in this work is recorded along the red and black lines shown in Figure 6a1 and b1. The different colours presented in Figure 6a1 represent different level of altitudes. At the initial state, light blue colour is observed along the width of the horizontal tows. Dark blue colour is observed between these ones. As globally, two colours are observed; a square periodic profile of tow elevation is obtained by processing the fringe projection measurements along the vertical line (Figure 6a2). This is due to the nature of the plain weave fabric manufactured with flat tows interlaced following a plain weave pattern (Figure 6a3). By performing approximate measurements

with a Vernier calliper directly on the fabric, it appears that the differential elevation between the warp and the weft tows is about 0.4 ± 0.1 mm.

At a state where buckles are well visible, the same procedure has been used. A colour gradient can be observed across the width of the horizontal tows (Figure 6b1). The altitude of the tow where buckles are formed show increasing altitude colours from one side of the tow to the other one up to a maximum value. A chevron type profile as presented in Figure 6b2 is well in accordance with the colour evolution and with the experimental observation (Figure 6b3). The maximum elevation recorded using the fringe projection technique has been compared with the one measured on the shape using a Vernier calliper. The measured altitude (1.55 ± 0.07 mm) is in good agreement with the ones given by the fringe projection technique.
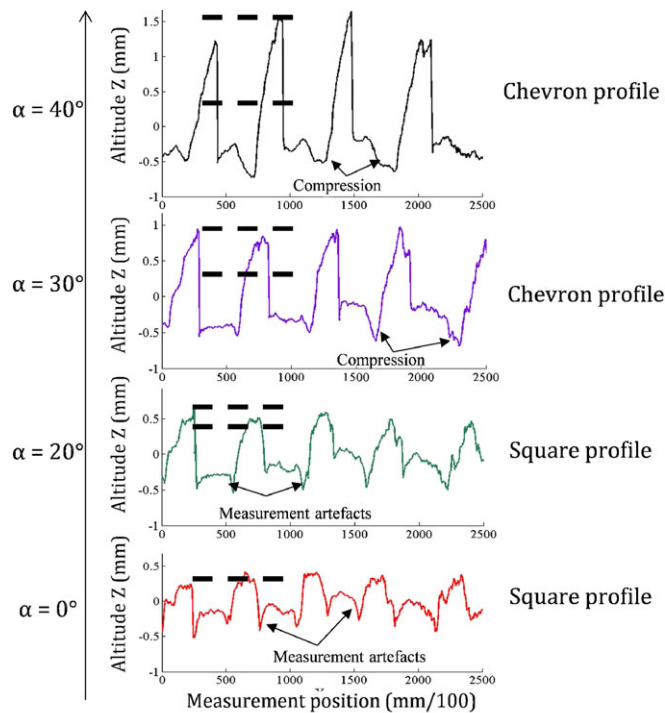
This preliminary test therefore indicates that the fringe projection technique, and the chain associated to the signal processing is validated. As a consequence, the profile evolution can be used to investigate into details the appearance and the growth of the buckles in the following section.
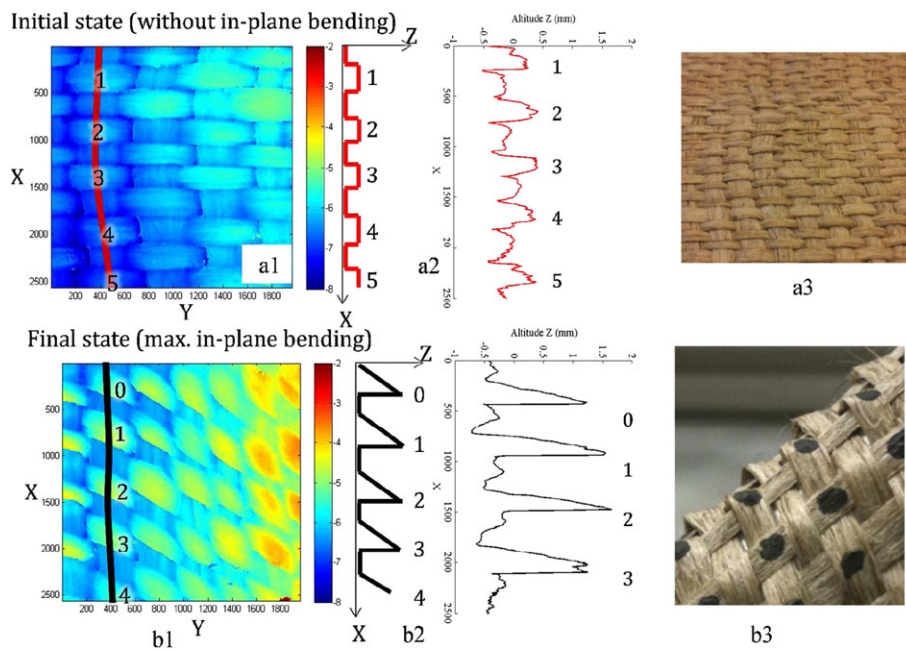
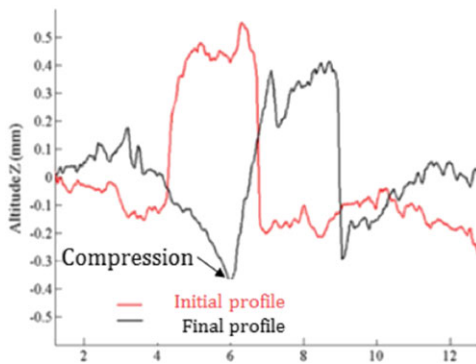**Figure 6:** Expected profile of the buckles

Profile of the buckles: evolution as a function of the in-plane bending angle

Figure 7a shows the evolution of the buckle's profile and altitude for four different in-plane bending angles. The colours presented in Figure 6a1 have been processed through in house MATLAB routines in order to get access to the actual elevation values.

The buckle's profile progressively changes from a square profile ($\alpha = 0°$) to a chevron type profile ($\alpha = 40°$) as observed on the edge of a tetrahedron shape (Figure 6b3). The change of the profile shape is progressive. A square type profile with different elevations than at the initial state is still observed for in-plane bending angle of 20°. For an in-plane bending angle of 30°, the square profile of the buckle disappears and is replaced by a chevron type profile. At the final state ($\alpha = 40°$), the profile remains similar, but the maximum elevation of the buckle is increased up to about 1.5 mm.

Figure 7a also shows that negative peaks of altitudes are observed before and after the rise of the buckles for each bending angle. These ones are due to the fact that the tow perpendicular to the one showing the buckle passes underneath it, and a drop of altitude is observed at its edge. However, the negative peak is more pronounced on the side of the buckle that does not show any altitude increase particularly for high value bending angles. This phenomenon is probably due to the fact that the tow exhibiting the buckle imposes a compression load on the tow passing underneath as a consequence of its rise. This phenomenon is due to the rotation of the buckle around itself in the buckle's zone as illustrated by a simple test on a single tow in Figure 8.

This phenomenon can also be observed on the profiles presented in Figure 7b for an orientation 90° of the fabric. The proportion of this negative decrease of altitude is actually larger in this case as no increases of altitude are observed between the initial and the maximum bending angle that the device can possibly impose. On the contrary, the altitude of the tow that still shows a square profile decreases. For high bending angles, a plateau of altitude is still observed, with a lower altitude. Even if the horizontal tows are submitted to equivalent bending angles, these ones do not show any increase of altitude like it is the case for the same test with a 0° orientation.

To study the profile evolution into details as a function of the increasing bending angle, the different recorded profiles have been aggregated. The bending angle at which the buckle appears for the orientation 0° can be investigated. The evolution of the profile is shown for increasing bending

(a): Orientation 0°

(b) Orientation 90°

Figure 7: Evolution of the buckles profile for different in-plane bending angles: (a) Orientation 0°, (b) orientation 90°
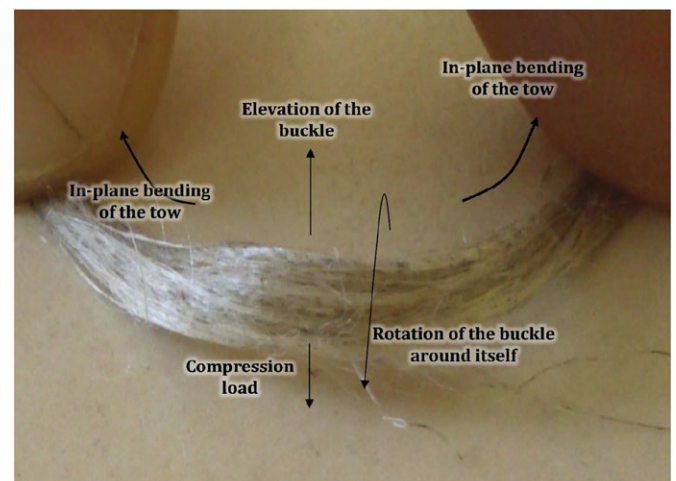

Figure 8: Rotation of the buckle around itself imposing a compression load

angles in Figure 9a for a sample placed with an orientation 0° (with the weft tows placed in a fixed position and warp tows submitted to in-plane bending) and in Figure 9b for a sample placed with an orientation 90°.

The maximum elevation of the buckle has also been recorded for each bending angles and is reported in Figure 10 for both orientations.

For the 0° orientation, it appears that low elevation is recorded below in-plane bending angles of 28°. For bending angles in the range [0–28°], the elevation slowly rises from its initial value (elevation 0.40 ± 0.04 mm) to reach a value of 0.6 mm. Above bending angles of 28° and up to 35°, an important rise of elevation is observed, from 0.6 to 1.45 mm. This is for our testing conditions (7.5 N and 15.3 N tensions applied in the X and Y directions) within this range of bending angle that the buckle rises in one side of the tow and decreases in altitude in the other side as described in Figure 8. For the highest bending angles tested in this work, the elevation still increases with a lower slope. It is also interesting to note that the full chevron profile is

not observed below angles of about 30°. This means that the buckle does not exhibit a continuous rising profile (chevron) for in-plane bending angles lower than about 30°. Up to this bending angle, the tow globally shows a plateau shape profile that progressively rises. Above 30°, instead of showing a plateau, the tow starts to rotate around itself and the buckle appears before quickly growing up to values of about 38°. Above this bending angle value, it probably becomes more difficult for the buckle to rise following a rotation around itself as this one needs to overcome compression resistance of the tow situated below it. The compression phenomenon and its magnitude are probably depending on the compression behaviour of the underneath tow as well as the lateral stiffness of the tow showing the buckle.

For the orientation 90°, an increase in altitude of the horizontal tow submitted to in-plane bending is observed up to about 28° (Figure 10). The altitude rise is very similar to the one observed for the 0° orientation up to this bending angle. However, above 28°, the altitude of the tow does not

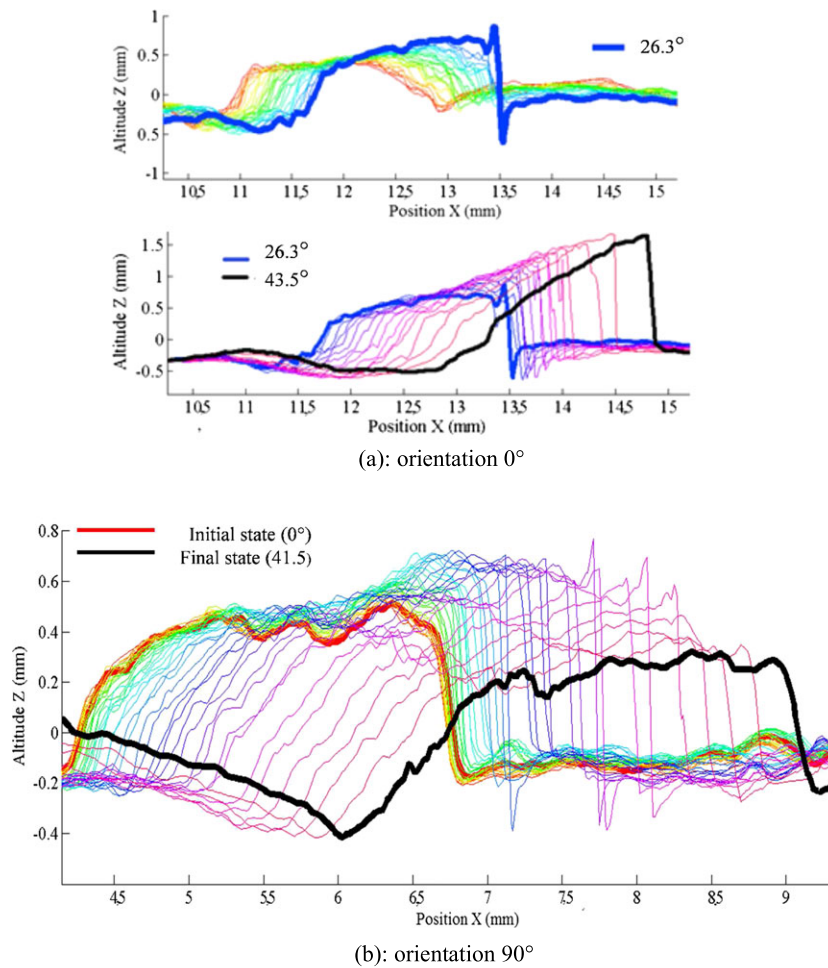
(a): orientation 0°

(b): orientation 90°

Figure 9: Profile evolution of a tow showing buckles: (a) orientation (0° with warp tows submitted to bending in its plane) and (b) orientation 90° with weft tows submitted to bending in its plane)
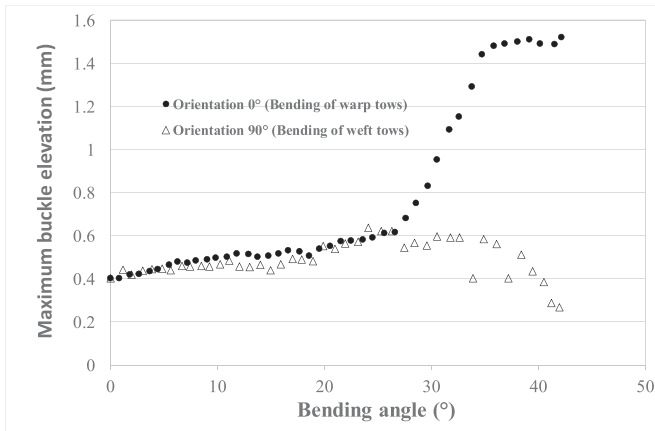
Figure 10: Maximum elevation of tows for different orientations of the plain weave fabric

rise anymore. It remains to a value of about 0.2 mm up to 38°. This elevation of altitude is visible on Figure 11. It shows that the tows submitted to in-plane bending do not keep their initial elevation. A small elevation with a square profile can be observed.

No appearance and growth of buckle with a rotation around itself takes place in these conditions. For the largest in-plane bending angles, the elevation of the horizontal tow decreases up to values of altitudes lower than the one of the initial state to reach an elevation of 0.22 mm. This corresponds to a decrease of about 45%. The fact that no buckle appeared with the orientation 90° is not really surprising as this had already been observed in a formed shape using the same plain weave fabric [16]. In the 90° orientation, the weft horizontal tows passes up and down the warp tows that are close to each other. The space between two adjacent warp tows is very small (0.26 mm). The length of the horizontal weft tow in the above position is therefore reduced to the width of the warp tows, 2.53 mm. This length is not sufficient for the buckle to appear in our test conditions. Moreover, the reduction of elevation for high in-plane bending angle is probably due to the fact that the tow, instead of rising to form a buckle imposes a compression load on the underneath warp tow.

Figure 11: Elevation of the weft tows submitted to in-plane bending solicitation: orientation 90°

On the contrary, for the 0° orientation, the space between two adjacent weft tows is larger (1.59 mm), and the width of the weft tows are larger (3.25 mm) than the warp tows. The length of the horizontal warp tow in the above position is therefore larger (about 4.8 mm). This is 1.9 times larger than for the weft tows.

The influence of the tension of the tows perpendicular to the ones exhibiting the buckles (vertical tows) has been also investigated. Figure 12 shows a comparison of the evolution of the buckles height as a function of the in-plane bending angle for orientation 0° for two different loadings (250 N and 8 N) in the X direction (direction of the tows perpendicular to the ones exhibiting the buckles) (Figure 3). In both cases, the global shapes of the curves are similar with a slow increase of the buckles height followed by an important rise and a plateau for the highest bending angles. However, in the case of the higher applied load in the X direction, the increase of the buckles height is observed for lower bending angles. The main rise starts from an in-plane bending angle of 20° instead of 28° in the case of the lower applied load. The final height of the buckle in both cases is equivalent (1.45 mm), but this height is reached for a lower angle, ~30° instead of 35° in the case of the low applied load in the X direction. This therefore means that a low tension in the X direction should be preferred if one want to delay the appearance of tow buckles in the frame of the fabric forming.

The variations of profile exposed in this work are the result of the buckle's appearance of the flax fabric tested in this work. It is expected that relatively similar behaviours are observed for other types of fabrics constituted from flat type tows. Buckles have already been observed on complex shapes elaborated from aeronautical grade carbon interlock fabric [25]. The profile of the buckles (presence of a plateau before the chevron full profile), their maximum elevation and the in-plane bending angle appearance depends on the different stiffness of the tow. Particularly, the lateral
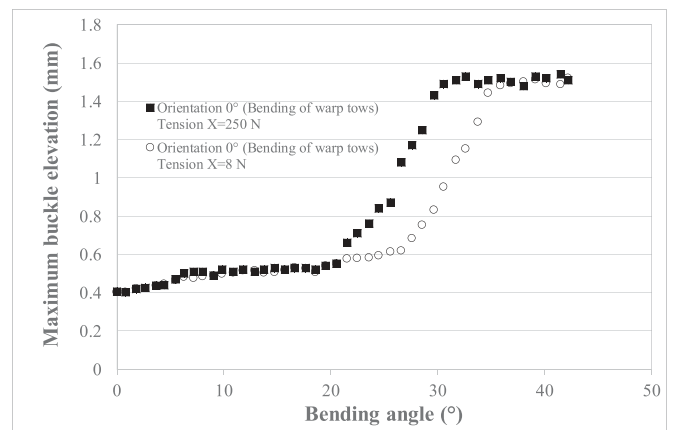

Figure 12: Influence of the tension in the tows perpendicular to the ones showing the buckles

stiffness of the tow probably controls the profile of the buckle. It would be expected that the chevron type profile is observed for lower bending angle in the case of tows with high lateral stiffness.

Conclusions

A device capable of reproducing tow buckles has been used to investigate the tow buckling phenomenon. Several techniques able to measure out of plane elevations have been discussed to detect the appearance and growth of the tow buckling phenomenon in relation to its size and its shape. The fringe projection technique was chosen as it gives the best compromise between the size of the defect to measure and its resolution. A complete description of the technique as well as the equipment used in this work is given.

The appearance and the growth of the tow buckle have been studied as a function of the in-plane bending angle that was identified as the essential parameter at the origin of the tow buckling phenomenon. For the reinforcement studied in this work, the tow supposed to show the buckle slowly rises up to an in-plane bending angle of 28°. The rise does not overcome the value of 0.2 mm. The profile of the tow remains with a square geometry. Above bending angles of 28°, the tow buckle itself appears (chevron profile), and its size quickly increases in the case of the orientation 0°. The tow buckle growth mechanism has been identified as a double rotation around itself. During its rotation, the tow exhibiting the buckle imposes a compression load on the tow underneath. Above a value of 35°, the buckle rises with a lower slope. This is due to the fact that the rotation around itself of the buckle is limited by the compression phenomenon taking place during this rotation.

As the plain weave fabric used in this study is not balanced, the 90° orientation was tested. In this case, the tow does not rise above a very limited value of 0.2 mm similarly to the orientation 0° up to in-plane bending angles of 28°. Above 28°, no more elevation is recorded. The tow does not rotate around itself as in the 0° case. This is due to the fact that the tow submitted to in-plane bending does not have enough space to initiate and grow a buckle. The space between two adjacent warp tows is very small (0.26 mm). The length of the horizontal weft tow in the above position is therefore reduced to the width of the warp tows (underneath in vertical position), 2.53 mm. This length is not sufficient for the buckle to appear in our test conditions.

If the in-plane bending angle is the main criterion at the origin of the tow buckle appearance and growth, it is not the only one. This work shows that the fabric architecture such as space between the tows perpendicular to the one showing the buckle is also crucial to control the buckle's appearance and growth.

The bi-axial state of the fabric (the tension of the horizontal and vertical tows) has been investigated. This work shows that the magnitude of the tension in the direction perpendicular to the tows showing the buckles is also a crucial parameter as a higher tension favours the appearance of buckles for lower in-plane bending angles. As one wants to avoid the appearance and the growth of the buckles, a low tension in the direction perpendicular to the one of the tows that may exhibit the buckles should be favoured. In this case, and with the tows and the reinforcement used in this work, an in-plane bending angle of 28° could be obtained in the face of a shape without any buckle appearance.

The characteristic in-plane bending angle values evaluated in this work probably also depend on the mechanical properties of the tows constituting the fabric. The compression stiffness of the tow underneath and the lateral compression of the tow showing the buckles are other parameters that probably influence the in-plane bending at which the buckle appears and then the speed at which it grows.

The influence of the fabric architecture at the mesoscale as well as the mechanical properties of the tow constituting the fabric and the bi-axial state of the fabric should be studied more by using the validated device to understand in a better extent the tow buckling defect. This would lead to tendencies that could be used to elaborate a multifactor criterion to predict the appearance and growth magnitude of the defect.

References

1. Potter, K., Khan, B., Wisnom, M., Bell, T., and Stevens, J. (2008) Variability, fibre waviness and misalignment in the determination of the properties of composite materials and structures. *Composites: Part A* **39**, 1343–1354.
2. A. C. Long. Composites Forming Technologies 2007 Woodhead Publishing Limited. ISBN: 978-1-84569-033-5.
3. Gereke, T., Döbrich, O., Hübner, M., and Cherif, C. (March 2013) Experimental and computational composite textile reinforcement forming: A review. *Composites: Part A* **46**, 1–10.
4. Bloom, L. D., Wang, J., and Potter, K. D. (2013) Damage progression and defect sensitivity: an experimental study of representative wrinkles in tension. *Composites: Part B* **45**, 449–458.
5. Lee, J., Hong, S., Yu, W., and Kang, T. (2007) The effect of blank holder force on the stamp forming behavior of non-crimp fabric with a chain stitch. *Compos. Sci. Technol.* **67**, 357–366.

6. Boisse, P., Hamila, N., Vidal-Sallé, E., and Dumont, F. (2011) Simulation of wrinkling during textile composite reinforcement forming Influence of tensile, in-plane shear and bending stiffnesses. *Compos. Sci. Technol.* **71**, 683–692.

7. Zhu, B., Yu, T. X., Teng, J., and Tao, X. M. (2009) Theoretical modeling of large shear deformation and wrinkling of plain woven composite. *J. Compos. Mater.* **43**, 125–138.

8. Ouagne, P., Soulat, D., Hivet, G., Allaoui, S., and Duriatti, D. (2011) Analysis of defects during the preforming of a woven flax. *Adv. Compos. Lett.* **20**, 105–108.

9. Pierron, F. (2008) Application of full-field measurement techniques to composite materials and structures. *Composites A* **39**, 1232–1244.

10. Lomov, S. V., Boisse, P., Deluycker, E., et al. (2008) Full-field strain measurements in textile deformability studies. *Composites A* **39**, 1232–1244.

11. Lomov, S. V., Ivanov, D. S., Verpoest, I., Zako, M., Kurashiki, T., Nakai, H., Molinard, J., and Vautrin, A. (2008) Full-field strain measurements for validation of meso-FE analysis of textile composites. *Composites: Part A* **39**, 1218–1231.

12. Willems, A., Lomov, S. V., Verpoest, I., and Vandepitte, D. (2009) Drape-ability characterization of textile composite reinforcements using digital image correlation. *Opt. Laser. Eng.* **47**, 343–351.

13. Lomov, S. V., Willems, A., Verpoest, I., Zhu, Y., Barburski, M., and Sotilova, T. (2006) Picture frame test of woven composite reinforcements with a full-field strain registration. *Text Res. J.* **76**, 243–252.

14. Cao, J., Akkerman, R., Boisse, P., et al. (2008) Characterization of mechanical behavior of woven fabrics: experimental methods and benchmark results. *Composites A* **39**, 1037–1053.

15. Pierce, R. S., Falzon, B. G., Thompson, M. C., and Boman, R. (June 2015) A low-cost digital image correlation technique for characterising the shear deformation of fabrics for draping studies. *Strain* **51**, 180–189.

16. Ouagne, P., Soulat, D., Moothoo, J., Capelle, E., and Gueret, S. (2013) Complex shape forming of a flax woven fabric; analysis of the tow buckling and misalignement defect. *Composites: Part A* **51**, 1–10.

17. Capelle, E., Ouagne, P., Soulat, D., and Duriatti, D. (June 2014) Complex shape forming of flax woven fabrics: Design of specific blank-holder shapes to prevent defects. *Composites: Part B* **62**, 29–36.

18. Walther, J., Simacek, P., and Advani, S. G. (2012) The effect of fabric and fiber tow shear on dual scale flow and fiber bundle saturation during liquid molding of textile composites. *Int. J. Mater. Form.* **5**, 83–97.

19. Arbter, R., Beraud, J. M., Binetruy, C., et al. (2011) Experimental determination of the permeability of textiles: a benchmark exercise. *Composites: Part A* **42**, 1157–1168.

20. Hou, Y., Comas-Cardona, S., Binetruy, C., and Drapier, S. (2012) Gas transport in fibrous media: application to in-plane permeability measurement using transient flow. *J. Compos. Mater.* . DOI:10.1177/0021998312455676.

21. Ouagne, P., and Bréard, J. (2010) Continuous transverse permeability of fibrous media. *Composites: Part A* **41**, 22–28.

22. Ouagne, P., Ouahbi, T., Park, C.-H., Bréard, J., and Saouab, A. (2012) Continuous measurement of fiber reinforcement permeability in the thickness direction: experimental technique and validation. *Composites: Part B* **45**, 609–618.

23. Davidson, P., Waas, A., Yerramalli, C., Chandrasekar, K., Faidi, W. (23–26 April 2012) Effect of Fibre Waviness on the Compressive Strength of Unidirectional Carbon Fibre Composites. 53rd structural materials comference, Honolulu, Hawaii.

24. Hayman, B., Berggreen, C., and Pettersson, R. (2007) The effect of face sheet wrinkle defect on the strength of FRP sandwich structures. *J. Sandwich struct. mater.* **9**, 377–404.

25. Allaoui, S., Hivet, G., Soulat, D., Wendling, A., Ouagne, O., and Chatel, S. (2014) Experimental preforming of highly double curved shapes with a case corner using an interlock reinforcement. *Int. J. Mater. Form.* **7**, 155–165.

26. Rozant, O., Bouban, P. E., and Manson, J. A. E. (2000) Drapability of dry textile fabrics for stampable thermoplastic preforms. *Composites: Part A* **31**, 1167–1177.

27. Launay, J., Hivet, G., Duong, A. V., and Boisse, P. (2008) Experimental analysis of the influence of tension on in-plane shear behaviour of woven composite reinforcements. *Compos. Sci. Technol.* **68**, 506–515.

28. Willens, A., Lomov, S., Verpoest, I., and Vandepitte, D. (2008) Optical strain fields in shear and tensile testing of textile reinforcements. *Compos. Sci. Technol.* **68**, 807–819.

29. Harrison, P., Clifford, M. J., and Long, A. C. (2002) Constitutive modelling of impregnated continuous fibre reinforced composites micromechanical approach. *Plast. Rubber Compos.* **31**, 76–86.

30. D'Agostino, M. V., Giorgio, I., Greco, L., Madeo, A., and Boisse, P. (2015) Continuum and discrete models for structures including (quasi-) inextensible elasticae with a view to the design and modelling of composite reinforcement. *Int. J. Solids Struct.* **59**, 1–17.

31. Dell'Isola, F., and Steigmann, D. (2015) A two-dimensional gradient-elasticity theory for woven fabrics. *J Elast* **118**, 113–125.

32. Ferretti, M., Madeo, A., dell'Isola, F., and Boisse, P. (2013) Modeling the onset of shear boundary layers in fibrous composite reinforcements by second-gradient theory. *Zeitschrift für angewandte Mathematik und Physik* 1–26.

33. Harrison, P. (2016) Modelling the forming mechanics of engineering fabrics using a mutually constrained panto-graphic beam and membrane mesh. *Composites: Part A* **81**, 145–157.

34. Kirkwood, J., Kuirkwood, K., Young, S. L., Egres, R., Wagner, N., and Wetzel, E. (2004) Yarn pull-out as a mechanism for dissipating ballistic impact energy in Kevlar KM-2 fabric. Part II: predicting ballistic performance. *Textile Res. J.* **74**, 939–948.

35. Heslehurst, R. B. (23–26 May 2011) Assessment of local damage in composite structures by optical methods. In: SAMPE Spring Technical Conference and Exhibition. Long Beach, CA, USA.

36. Ambu, R., Aymerich, F., Ginesu, F., and Priolo, P. (2006) Assessment of NDT interferometric techniques for impact damage detection in composite laminates. *Compos. Sci. Technol.* **66**, 199–205.

37. Crammond, G., Boyd, S. W., and Dulieu-Barton, J. M. (11 JUN 2015) A point-wise approach to the analysis of complex

composite structures using digital image correlation and thermoelastic stress analysis. *Strain*Article first published online: . DOI:10.1111/str.12142.

38. Wang, F., Xie, H., and Fulong, D. (February 1999) Qu Weibo measurement of strain concentration factor of composites plate using moiré interferometry. *Strain* **35**, 11–14.

39. Pezzoni, R., and Krupka, R. (2001) Laser-shearography for non-destructive testing of large area composite helicopter structures. *Insight* **43**, 244–248.

40. Abou-Khousa, M. A., Ryley, A. C., Kharkovsky, S., et al. (2007) shearography and through-transmission ultrasonic methods for inspection of honeycomb composites. In: Rev Prog QNDE: 26(Thompson, D. O., and Chimenti, D. E. Eds). Springer: 999–1006.

41. Post, D., Han, B., and Ifju, P. (1994) High Sensitivity Moire´: Experimental Analysis for Mechanics and Materials. Springer, Berlin.

42. Ibrahim, M. E. (September 2014) Nondestructive evaluation of thick-section composites and sandwich structures: A review. *Composites: Part A* **64**, 36–48.

43. Beakou, A., Cano, M., Le Cam, J. B., and Verney, V. (September 2011) Modelling slit tape buckling during automated prepreg manufacturing: A local approach. *Compos. Struct* **93**, 2628–2635.

44. Tephany, C., Gillibert, J., Ouagne, P., Hivet, G., Allaoui, S., and Soulat, D. (2016) Development of an experimental bench to reproduce the tow buckling defect appearing during the complex shape forming of structural flax based woven composite reinforcements. *Composites: Part A* **81**, 22–33.

45. Hariharan, P. (2006) Basics of Interferometry. 2nd edn. Academic Press.

46. Leandry, I. (2012) Adaptation de la Méthode Deprojection de Franges pour la Mesure du Relief de Grands Objets et Pour la Modelisation Anthropometrique: Application à l'étude de Flotteurs sous Pression et au Suivi de Pathologie de L'abdomen. PhD thesis, University of Poitiers, France.

47. Surrel, Y. (2014) Les techniques optiques de mesure de champ: essai de classification. *Instr. Mes. Metr.* **4**, 11–42.

48. Jahne, B., Geeissler, P., and Haussecker, H. (1999) Handbook of Computer Visional Applications-Volume 1 : Sensors and Imaging. 1st edn.Morgan Kaufmann Publishers Inc., San Francisco, CA, USA.

49. Gorthi, S. S., and Rastogi, P. (2010) Fringe projection techniques: Whither we are. *Opt. Lasers Eng.* **48**, 133–140.